LS Note No. 202
April, 1992

Digital Signal Processing for Beam Position Feedback

Y. Chung, L. Emery, and J. Kirchman
Advanced Photon Source
Argonne National Laboratory
Argonne, IL 60439

Abstract

Stabilization of the particle beam position with respect to the focusing optics in the third generation synchrotron light sources is crucial to achieving low emittance and high brightness. For this purpose, global and local beam orbit correction feedbacks will be implemented in the APS storage ring. In this article, we will discuss application of digital signal processing to particle/photon beam position feedback using the PID (proportional, integral, and derivative) control algorithm.

1. Introduction

In the third generation synchrotron light sources, of which the Advanced Photon Source is one, it is very important to stabilize the beam position on the magnetic axis of the quadrupoles and the sextupoles in order to achieve low emittance and high brightness of the photon beams. A number of correction dipole magnets will be installed around the APS storage ring to stabilize the beam against the low frequency vibration, below 25 Hz, from various sources. The corrector magnet system will consist of 318 vertical/horizontal field magnets for horizontal and vertical corrections.

The displacement of the quadrupole magnets due to vibration has the most significant effect on the stability of the positron closed orbit in the storage ring. A small displacement of the quadrupole magnet leads to a large distortion of the closed orbit, and hence, the growth of the emittance. The internal sources of vibration include the mechanical motion of the various components of the ring, such as rotating machinery, pumps, compressors and high vacuum equipment. This internal vibration can be reduced by balancing the equipment and isolating the sources. The primary external source of the low frequency vibration is the ground motion of maximum 20 μm amplitude, with frequency components concentrated below 10 Hz. These low frequency vibrations can be corrected using the corrector magnets, whose field strengths are controlled individually through the feedback loop comprising the beam position monitoring (BPM) system.[1]

For the global beam position feedback, the beam motion is detected by the BPMs located around the storage ring, and is relayed in digital format from the BPMs to several feedback processors. The feedback processors compare the current positions and the desired positions set by the control system and compute the necessary kick strengths for the corrector magnets to restore the beam to the desired positions. The feedback processors then send commands to individual corrector magnet power supplies. The corrected beam positions will then be measured by the BPMs and the feedback loop continues.

In order to take advantage of the digital interface on the BPM system and the power supplies on the APS, the feedback loops will be implemented using digital signal processing (DSP),

except for the analog front end of the BPM processing electronics. This will render the feedback system immune to the RF noise, signal deterioration over the transmission line, and other problems which characterize analog circuits.

A noteworthy advantage of DSP over the analog circuits is the design of the compensation filter for the eddy current in the vacuum chamber. Even though the eddy current effect may be described by a simple multipole low–pass filter within the bandwidth of interest, designing a corresponding high–pass filter which cancels the eddy current effect is not simple. However, it is relatively easy to design a digital filter using the Z–transform once the transfer function of the vacuum chamber to the AC magnet field is known.

The remainder of this article consists of four sections. In Section 2, we will briefly describe formulation of DSP using Z–transform and discuss the design of digital filters using analytical formula and data from measurements on analog devices. In Section 3 the digital feedback using the PID control algorithm will be described, and in Section 4 we will discuss its application to global and local beam position feedback. A summary and suggestions for future work will be presented in Section 5.

2. Formulation of Digital Signal Processing

Digital signal processing is now a mature field in the theory of controls and a large body of literature is available. Since we are interested in the application of DSP rather than development of a new theory, we will outline in this section the principles and results found in Ref. 2. Then we will discuss the application of DSP to the open loop compensation for the eddy current effect in the vacuum chamber. This compensation filter will be incorporated in the closed loop feedback system as discussed in Sections 3 and 4.

2.1 Z–transform and Digital Filters

Just as the Fourier transform and the Laplace transform are important in continuous–time signals and systems, Z–transform facilitates the analysis of discrete–time signals and systems. Given a sequence of discrete–time signals $\{x_n\}$, its Z–transform is defined by

$$X(z) = \sum_{n=-\infty}^{\infty} x_n z^{-n} \tag{2.1}$$

where z is a complex variable and plays a role similar to that of the variable s in the Laplace transform. $\{x_n\}$ is called the inverse transform of X(z).

A large class of linear time–invariant discrete–time systems can be described by the linear constant coefficient difference equation

$$y_n = \sum_{k=0}^{M} a_k x_{n-k} - \sum_{k=1}^{L} b_k y_{n-k}\,, \tag{2.2}$$

where $\{x_n\}$ is the input, $\{y_n\}$ is the output, and $a_0, a_1, \ldots, a_M, b_1, \ldots, b_L$ are constants that characterize the system. A digital filter with $b_k = 0$ for all values of k is called a finite impulse response (FIR) filter. Otherwise, it is called a infinite impulse response (IIR) filter. Applying the Z–transform to Eq. (2.2), we obtain

$$Y(z) = H(z)X(z) \tag{2.3}$$

where

$$H(z) = \frac{\sum_{k=0}^{M} a_k z^{-k}}{1 + \sum_{k=1}^{L} b_k z^{-k}} . \tag{2.4}$$

X(z) and Y(z) are the Z–transforms of $\{x_n\}$ and $\{y_n\}$ and H(z) is the transfer function of the filter.

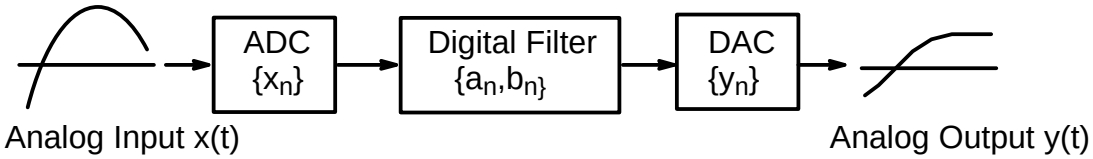

Fig. 2.1: Processing of an analog signal using a digital filter.

The Z–transform in Eq. (2.1) is closely related to the Fourier transform. Consider applying the digital filter represented by the coefficients $\{a_n, b_n\}$ to processing of an analog signal as shown in Fig. 2.1. Suppose the sequence $\{x_n\}$ was obtained by digitally sampling an analog signal x(t) with a sampling rate of $F_s = 1/T$, and let $X^a(\omega)$ be the Fourier transform of x(t). We will call ω the analog frequency. Now, let us introduce the digital frequency λ, which has the range $(-\pi, \pi)$. Using $x_n = x(nT)$ in Eq. (2.1) with $z = e^{-i\lambda}$, it can be shown that

$$\begin{aligned} X(e^{-i\lambda}) &= \sum_{n=-\infty}^{\infty} x(nT)\, e^{in\lambda} \\ &= F_s \sum_{k=-\infty}^{\infty} X^a(F_s(\lambda + 2\pi k)) \ . \qquad (-\pi < \lambda < \pi) \end{aligned} \tag{2.5}$$

Equation (2.5) is the relation between the analog spectrum $X^a(\omega)$ and the digital spectrum $X(e^{-i\lambda})$, which exhibits a periodicity of 2π in λ. Suppose the original signal x(t) was properly bandlimited such that

$$X^a(\omega) = 0, \qquad |\omega| > \pi F_s \, , \tag{2.6}$$

then the various terms in the summation in Eq. (2.5) are non–overlapping. However, as the sampling frequency decreases below the level at which Eq. (2.6) holds, overlapping will increase and cause aliasing error. Therefore the sampling frequency F_s determines the degree of overlapping among the various components in the summation in Eq. (2.5) and must be determined carefully for a given input signal. The minimum sampling frequency for which Eq. (2.6) holds is called the Nyquist frequency.

Given the output sequence $\{y_n\}$, the analog spectrum $Y^a(\omega)$ from the reconstruction filter with the sampling time $T = 1/F_s$ can be expressed as

$$Y^a(\omega) = G(\omega) Y(e^{-i\omega T}) \, . \tag{2.7}$$

$G(\omega)$ is the frequency characteristic of the reconstruction filter, which has the time response g(t) such that

$$\int_{-\infty}^{\infty} dt\ g(t) = G(0) = T\,. \tag{2.8}$$

Therefore, using Eq. (2.5) and the relation $Y(z) = H(z)X(z)$, we obtain

$$Y^a(\omega) = F_s G(\omega) H(e^{-i\omega T}) \sum_{k=-\infty}^{\infty} X^a(\omega + 2\pi k F_s)\,. \tag{2.9}$$

The role of the reconstruction filter $G(\omega)$ is to eliminate the undesirable high frequency components in the summation of Eq. (2.5). Ideally, a filter that has the frequency characteristic

$$G(\omega) \approx \begin{cases} T & |\omega| < \pi F_s \\ 0 & |\omega| > \pi F_s \end{cases} \tag{2.10}$$

should be used. Assuming the sampling frequency F_s to be larger than the Nyquist frequency so that there is no significant overlap in the summation of Eq. (2.9), we have

$$Y^a(\omega) \approx \begin{cases} H(e^{-i\omega T}) X^a(\omega) & |\omega| < \pi F_s \\ 0 & \text{otherwise} \end{cases} \tag{2.11}$$

This is the fundamental relation for the digital filtering of analog signals. It shows that the digital filter transfer function $H(z)$ performs the spectral modification of the input signal $x(t)$. From Eqs. (2.5) and (2.11), we find that the digital frequency λ is related to the analog frequency ω by

$$\lambda = \omega T. \tag{2.12}$$

The design of digital filters can be broadly categorized into two classes and proceeds as follows. In one case, the design is based on an analog filter with known frequency characteristics with an appropriate analog frequency to digital frequency transformation $\omega = \omega(\lambda)$. When the analytic form of the corresponding analog filter transfer function $H^a(\omega)$ is known, a proper frequency transformation between ω ($-\infty < \omega < \infty$) and λ ($-\pi < \lambda < \pi$) is found first. Then from $z = e^{-i\lambda}$, ω can be expressed in terms of z, and the digital filter transfer function $H(z)$ is obtained by substituting ω with $\omega(z)$ in $H^a(\omega)$. The reason for doing this is that the relation between λ and ω in Eq. (2.12) is not always the convenient form to work with, since an analog filter transfer function $H^a(\omega)$ which is rational in ω will produce a digital transfer function $H(z)$ which is not rational in z^{-1} as shown in Eq. (2.4).

In the other case, when only $|H^a(\omega)|$ is known at various frequencies, a computer–aided method is applied to obtain $H(z)$ in the factored form (cascade form). In the following subsections, we will show some examples of digital filter design and its application to the open loop compensation for the eddy current in the APS storage ring vacuum chamber.

2.1 Low–Pass Filter

In this subsection, we will consider a low–pass filter characterized by the transfer function

$$H^a(\omega) = \frac{\omega_c}{\omega_c - i\omega}\,, \tag{2.13}$$

where ω_c (= $2\pi f_c$) is the angular cutoff frequency and is the inverse of the decay time τ. We chose this function for later use on bandlimiting the closed loop feedback. To transform ω to the digital frequency λ, we use

$$\omega \tan\left(\frac{\Lambda_c}{2}\right) = \omega_c \tan\left(\frac{\lambda}{2}\right) \tag{2.14}$$

From Eq. (2.12), Λ_c is given by

$$\Lambda_c = \omega_c T . \tag{2.15}$$

This will map the range $(-\pi, \pi)$ of λ into $(-\infty, \infty)$ of ω, and when ω is equal to ω_c, λ is equal to Λ_c. When ω_c is much smaller than the sampling frequency, that is, $\omega_c << F_s$, the relation $\lambda = \omega T$ is restored. Inserting Eq. (2.14) into Eq. (2.13) and using $z = e^{-i\lambda}$, we obtain

$$H(z) = H^a(\omega(z)) = \frac{1 + z^{-1}}{1 + c + (1 - c)z^{-1}}, \qquad c = \cot\left(\frac{\Lambda_c}{2}\right). \tag{2.16}$$

This is an infinite impulse response (IIR) filter. From Eq. (2.4), we obtain

$$a_0 = \frac{1}{1 + c}, \; a_1 = \frac{1}{1 + c} \text{ and } b_1 = \frac{1 - c}{1 + c}. \tag{2.17}$$

The digital filter obtained by substituting these coefficients in Eq. (2.2) will have the characteristic of a low–pass filter of bandwidth f_c.

2.2 Computer–Aided Design of Digital Filters

When an analytic form for the desired transfer function is not known, we must resort to a numerical method to find out the filter coefficients, a's and b's, from amplitude responses specified for the filter. Given a set of amplitude responses A_n, $1 \le n \le N$, for digital frequencies λ_n, we will obtain the transfer function in the form

$$H(z) = C \prod_{k=1}^{K} \frac{1 + f_k z^{-1} + g_k z^{-2}}{1 + c_k z^{-1} + d_k z^{-2}}. \tag{2.18}$$

where the real constants C, c_k, d_k, f_k, g_k, $(1 \le k \le K)$ are to be determined, so that the amplitude of the resulting H(z) approximates A_n at $z_n = e^{-i\lambda_n}$ as closely as possible. The algorithm for finding these constants is described in Ref. 2, together with the source code for the computer program.

2.3 Digital Compensation of Analog Filters

In the previous section we discussed the analog characteristic of signals processed by a digital filter and it was shown that a digital filter can be designed such that its response closely matches that of an analog filter. Since multiple digital filters connected in series can be represented by the product of the corresponding transfer functions as seen from Eq. (2.3), it is possible to design a digital filter which is the reciprocal of a given analog filter. Suppose H(z) is the transfer function of an analog filter in z–space, which is written as in Eq. (2.4). Then a digital filter with the transfer function equal to $H(z)^{-1}$ given as

$$H(z)^{-1} = \frac{1}{a_0} \frac{\sum_{k=0}^{L} b_k z^{-k}}{1 + \sum_{k=1}^{M} \frac{a_k}{a_0} z^{-k}} \qquad (b_0 = 1) \qquad (2.19)$$

will closely cancel the effect of the analog filter, so that the combination of the two filters equals unity.

A digital compensation filter is useful in the application of the closed loop feedback with an analog device with frequency–dependent attenuation (or gain) and phase shift. Large attenuation of the signal decreases the open loop gain and the effectiveness of the feedback, and a large phase shift exceeding 90° can make the feedback loop oscillatory or unstable. By canceling out these two effects, a digital compensation filter inserted in front of the offending analog device will make the feedback loop much more effective and stable.

One such example is the effect due to the eddy current in the vacuum chamber, which flows in the direction canceling the original magnet field and decreases not only the field inside the vacuum chamber but also the field outside in the vicinity of the vacuum chamber. The corrector magnet field controlling the beam position is strongly attenuated and shifted in phase, which could result in oscillatory behavior or loss of the stored beam.

3. Closed Loop Feedback with DSP

In designing the digital signal processing scheme for closed loop feedback, the following factors must be considered.

- Rise–time
- Overshoot
- Settling time
- Control effort
- Noise throughput

The rise–time of the output signal from the feedback loop in response to the input step pulse is related to the bandwidth of the control, and generally the shorter the rise–time, the better. However, a short rise–time can lead to overshoot in the output, and a compromise is needed to balance the two. This can be achieved by limiting either the controller gains or the slew rate of the output, which, in effect, is tantamount to limiting the bandwidth.

The closed loop feedback control can also produce oscillation or ringing in the output with a finite settling time. This is generally the result of too low a sampling frequency compared to the bandwidth of the input or the noise. It also depends on the structure of the feedback scheme. Ideally, the sampling frequency should be large enough such that the output from the feedback loop is critically damped in response to the input step pulse.

The control effort is the signal applied to the device to be controlled. For beam position feedback, it will be the output voltage or current of the corrector magnet power supply. This factor must be considered together with the spectrum and the desired throughput of the noise in determining the controller gains and the bandwidth of the feedback loop.

The four parameters discussed above, the controller gains, bandwidth, sampling frequency, and the structure of the feedback scheme, determine the performance of the closed loop feedback. In the following sections, we will discuss these parameters and the application of closed loop feedback to the beam position control using DSP.

3.1 Digital Signal Processing Using PID Control

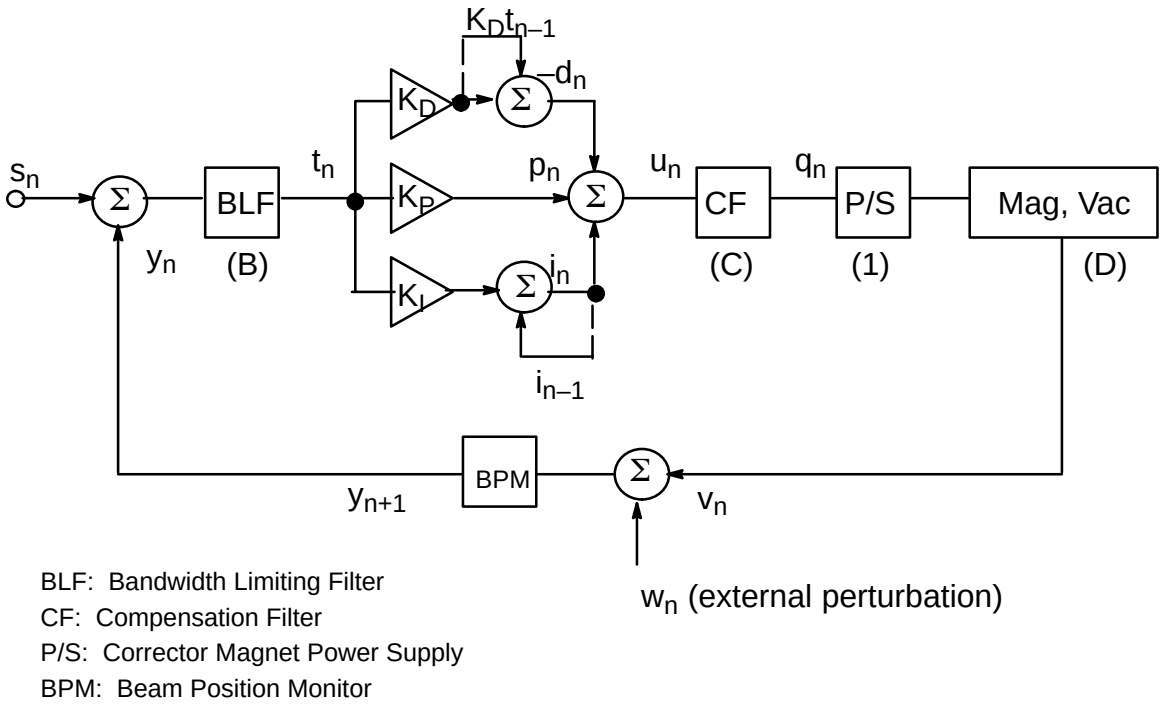

BLF: Bandwidth Limiting Filter
CF: Compensation Filter
P/S: Corrector Magnet Power Supply
BPM: Beam Position Monitor

Fig. 3.1: Schematic diagram for the closed loop feedback with PID control.

In this section, we will analyze the PID (proportional, integral, and derivative) control. In Fig. 3.1 is shown the schematic diagram for PID control. The various symbols (s_n, y_n, t_n, u_n, v_n, w_n, p_n, i_n, d_n) denote the digital signals that corresponds to the n–th cycle. s_n is the control signal for the desired beam position and y_n is the measured beam position. The error signal $s_n - y_n$, after being passed through a digital band limiting filter with transfer function B(z), is modified by the three controllers, proportional, integral, and derivative. For stability reasons, the band limiting filter is a single–pole low pass filter. This signal is passed through another digital filter which compensates for the effect of the magnet and the vacuum chamber. The corrector magnet is activated accordingly and external perturbation w_n is added to the beam position. One feedback cycle ends with the reading of new beam position y_{n+1}. In the following discussion, we assume for simplicity that the magnet and vacuum chamber effects are exactly canceled by the compensation filter, that is, CD = 1, and that the transfer function of the power supply is equal to unity.

The controller gains K_P, K_I, and K_D, are yet to be determined to satisfy the feedback control specifications. In order to find the overall transfer function of the feedback loop, we write the relations between the z–transforms of various signals as they pass through each component. Let S(z) be the z–transform of $\{s_n\}$, Y(z) the z–transform of $\{y_n\}$, and so forth. Then we have

$$
\begin{gathered}
T(z) + B(z)\ (S(z) = Y(z))\,, \\
U(z) = T(z)\left(K_P + K_D(1 - z^{-1}) + \frac{K_I}{1 - z^{-1}}\right), \\
zY(z) = U(z) + W(z)\,.
\end{gathered}
\tag{3.1}
$$

From these relations, we obtain

$$
Y(z) = \frac{F(z)B(z)}{z + F(z)B(z)}S(z) + \frac{1}{z + F(z)B(z)}W(z)\,. \tag{3.2}
$$

where

$$
F(z) = K_P + K_D\ (1 - z^{-1}) + \frac{K_I}{1 - z^{-1}}\,. \tag{3.3}
$$

Equation (3.3) is the expression for the output from the closed loop feedback using PID control with the control signal S(z) and the perturbation W(z). At DC with finite K_I, F(z) becomes infinitely large and the noise transfer function Y(z)/W(z) with S(z) = 0 is equal to 0, which is the characteristic of the integral control. However, the gain parameter K_I must be kept small to prevent oscillation in the output. The control action in the medium and high frequency regions is dominated by the proportional and derivative control terms. The derivative control term is zero at DC, and increases to $2K_D$ as the digital frequency λ approaches π.

Figure 3.2 shows the amplitude and phase of the noise transfer function with PID control with parameters $K_P = 5$, $K_I = 0.25$, $K_D = 2$, $F_s = 4$ kHz, and $f_b = 30$ Hz. At 20 Hz, the noise is attenuated by 17.9 dB and the phase is advanced by 83°, while at 60 Hz, the noise is attenuated by 8.5 dB and the phase is advanced by 67°. The response of the feedback loop when a step impulse is applied to the control signal is shown in Fig. 3.3, using the same parameters as in Fig. 3.2. The rise time at 90% of the control level is approximately 2 msec. The output y(t) shows neither noticeable overshoot after the initial rise nor oscillation while settling to the control level.

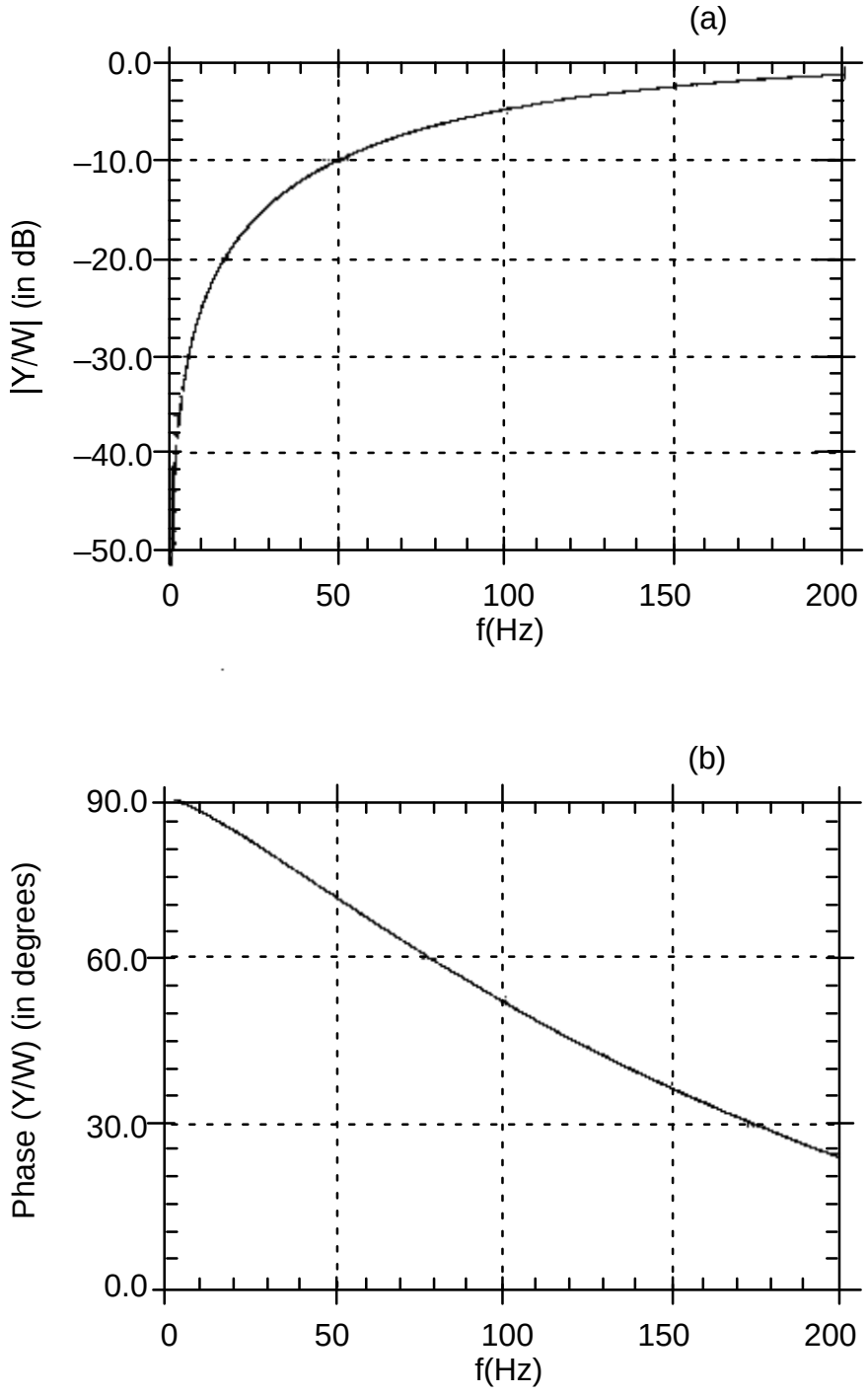

Fig. 3.2: Noise transfer function Y(z)/W(z) with S(z) = 0 as a function of frequency for closed loop feedback using PID control: (a) amplitude and (b) phase. The parameters used were: $K_P = 5$, $K_I = 0.25$, $K_D = 2$, $F_s = 4$ kHz, and $f_b = 30$ Hz.

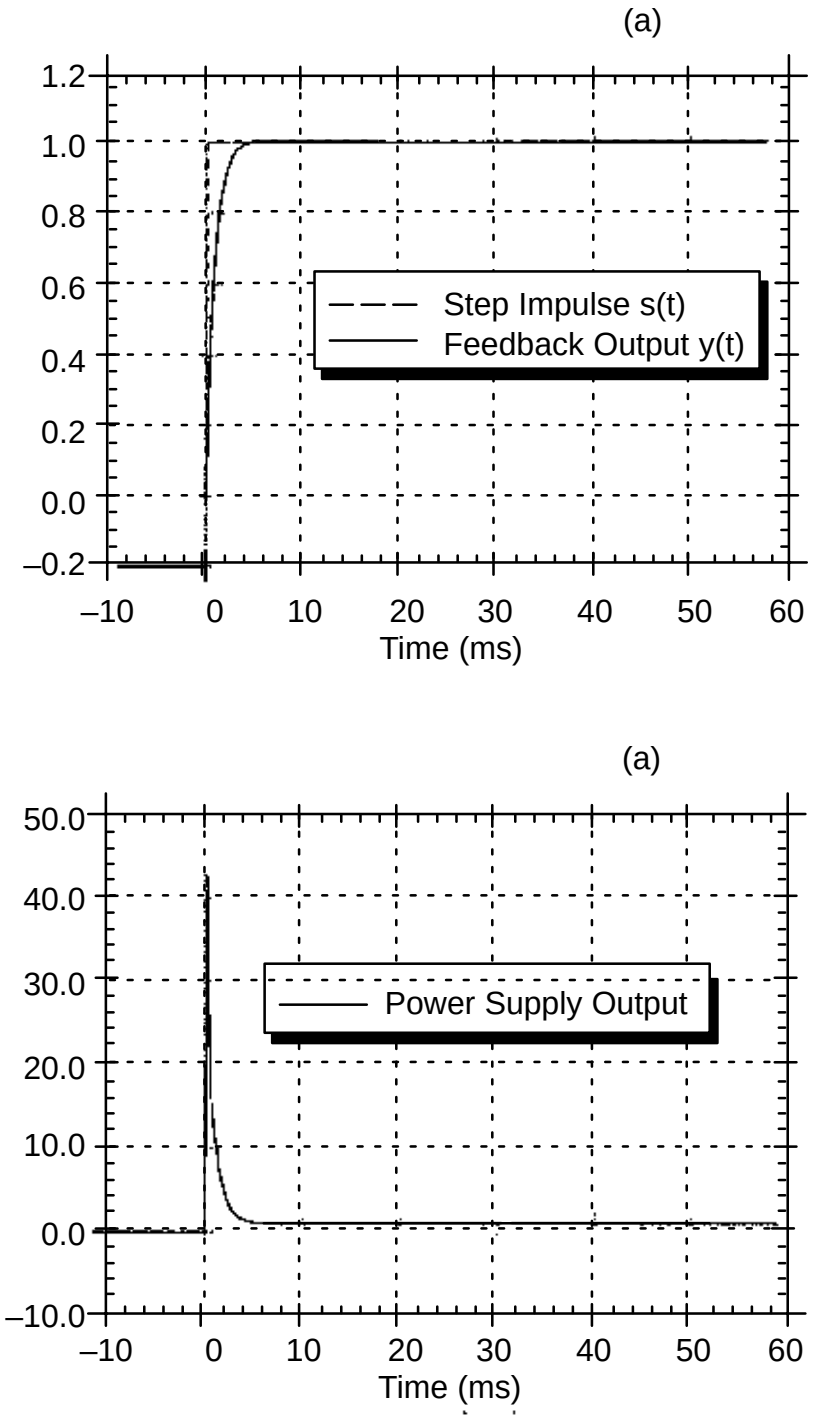

Fig. 3.3: Step impulse response using PID control. (a) shows the response of the feedback loop to control step impulse. (b) shows the required power supply output for a 5 Hz bandwidth load. The parameters used were: $K_P = 5$, $K_I = 0.25$, $K_D = 2$, $F_s = 4$ kHz, and $f_b = 30$ Hz.

However, a very robust power supply is required if the bandwidth of the device under control is small, such as a corrector magnet and vacuum chamber. This is due to the action by the compensation filter feeding the power supply control input. Figure 3.3(b) shows the required

power supply output as a function of time if the bandwidth of the load is 5 Hz. The peak output immediately after the step impulse is 42.7 in units of the control level.

4. Beam Position Feedback

Both the global and local correction schemes will be used to stabilize the positron and photon beams. The global correction reduces the orbit everywhere around the ring using several correctors (about 40). The local correction consists of bumps in the photon source regions. The orbit is expected to be almost fully corrected at these locations. Both global and local correction will have the same bandwidth, since the correctors employed have the same frequency characteristics. In the following discussion we will assume that the local feedback loops are decoupled from each other and from the global feedback loop. In reality, this is not true, and imperfect isolation of the local feedback loops will lead to interference and deterioration of the orbit stability.

If corrector strengths were unlimited, one would need to operate only local bump feedback to stabilize the photon beam. Since we do not care what happens to the electron orbit outside the local bumps (as long as the orbit allows good enough lifetime), the global correction could be omitted. However, including a global correction will always partly relieve the burden of the local bump correction. For instance, the global correction could be specified to remove 80% of the distortion around the ring, including the photon source regions. Therefore, a local bump correction specified to correct a 100–μrad 25–Hz orbit distortion would be sufficient in a ring where the orbit motion at 25 Hz is of the order of 500 μrad. The parameters for the global and local correction systems are listed in Table 4.1.

4.1 Global Feedback

Displacement of the particle beam position due to a kick of $\Delta y_c'$ by a corrector magnet is given by[3]

$$y = \Delta y_c' \frac{\sqrt{\beta_c \beta}}{2 \sin(\pi\upsilon)} \cos\left(|\phi - \phi_c| - \pi\upsilon\right), \tag{4.1}$$

where β is the beta function at the beam position monitor observing the beam motion y, $\Delta y_c'$ is the angular deflection caused by the corrector magnet, and β_c is the beta function at the corrector magnet. ϕ and ϕ_c are the betatron phase at the beam position monitor and the corrector magnet, respectively, and ν is the tune. Equation (4.1) relates the corrector strength and the beam displacement, both of which are measurable. Since the angle of deflection $\Delta y_c'$ is proportional to the magnetic field in the vacuum chamber, the beam position x_i measured by the i–th beam position monitor and the corrector magnet field B_j inside the vacuum chamber are linearly related. From Fig. 3.1, we see that B_j is also proportional to the signal u_n, which is modified by the compensation filter to cancel the effect of the vacuum chamber eddy current before being sent to the magnet power supply controller.

Table 4.1: Specification of the beam position correction systems.

	Global DC	Global AC	Local
Orbit measurement device	All of the RF BPMs	RF BPMs at sources only	X–ray photon BPMs
Correctors	All correctors	Subset of correctors	Local bump
Specified orbit measurement resolution	25 μm	25 μm	Not specified
Achievable resolution	5 μm	5 μm	1 μm
Required range of orbit correction	± 20 mm	± 500 μm	± 100 μm

Using the notation of Section 3, we write

$$v_n^i = Q_j^i u_n^j \ . \qquad (1 \le i \le M,\ 1 \le j \le N,\ \text{summation over j}) \tag{4.2}$$

or, in vector notation,

$$\mathbf{v}_n = \mathbf{Q} \cdot \mathbf{u}_n \ . \tag{4.3}$$

The indices i and j denote the i–th BPM and the j–th corrector magnet, respectively. We will assume that there are unequal numbers of BPMs (total of M) and corrector magnets (total of N). The matrix **Q** is a constant matrix, has dimensions M × N and represents the correlation between the corrector magnet strengths and the beam motion at selected BPM locations. The elements of **Q** can be obtained by measuring the beam motion y^i with given DC signal u^j, assuming that the noise w^i is negligible compared to y^i.

Equation (4.2) indicates that the correction of beam position at a given location is the result of a simultaneous action by N corrector magnets. Now that there are M such BPM locations where the desired beam positions are specified, a set of linear equations like Eq. (4.2) needs to be solved to obtain the strength for N corrector magnets. This is equivalent to inverting the matrix **Q** and can be done by using the well–known technique of "singular value decomposition (SVD)".[4] This technique will allow us not only to solve for the corrector magnet strengths but also to know in advance whether a given set of BPMs and corrector magnets render the matrix **Q** singular or not.

When M ≤ N, there exists a matrix **R** of dimensions N × M that pseudo–inverts **Q**. That is,

$$\mathbf{Q} \cdot \mathbf{R} = \mathbf{1} \, , \tag{4.4}$$

where **1** is a unit matrix of dimensions M × M. In this case the BPMs are decoupled from each other and it is possible to control the beam position at each BPM independently. While the matrix **R** is not necessarily unique, SVD picks the matrix that corresponds to the minimum control effort.

On the other hand, when M > N, the pseudo–inverse matrix **R** obtained using SVD does not satisfy Eq. (4.4). It simply guarantees that the difference $\left| \mathbf{Q} \cdot \mathbf{R} \cdot \mathbf{t} - \mathbf{t} \right|$ for an arbitrary vec-

tor **t** is at its minimum. In this case, the BPMs are not decoupled from each other and it is in principle impossible to control beam position at individual BPMs. The coupling between BPMs could also degrade the closed loop stability. For this reason, the use of more BPMs than corrector magnets for global beam position feedback is not recommended.

Since the location of the matrix **R** determines the number of PID controllers and compensation filters (CF), and therefore, the turnaround time of the feedback loop, the dependence of the these components on corrector magnets and vacuum chamber and the relative sizes of M and N must be considered in deciding where to put **R**. If M < N, **R** is placed in front of the compensation filter (CF), and if M ≥ N, **R** is placed after the last channel–dependent component. The bandlimiting filter should still precede **R** in order to minimize the possibility of overflow during computation. Basically, this follows from Eq. (4.4) and the fact that the matrix **R** transforms the M input channels from the BPMs into the N output channels to the corrector magnets. Assuming that the bandlimiting filter and the PID controllers are the same for all input channels, we obtain a relationship similar to Eq. (3.2) for M ≤ N,

$$Y^i(z) = \frac{F(z)B(z)}{z + F(z)B(z)}\ S^i(z) + \frac{1}{z + F(z)B(z)} W^i(z)\ . \qquad (1 \le i \le M) \quad (4.5)$$

In Fig. 4.1 is shown an example of such an arrangement for M = 4 and N = 8.

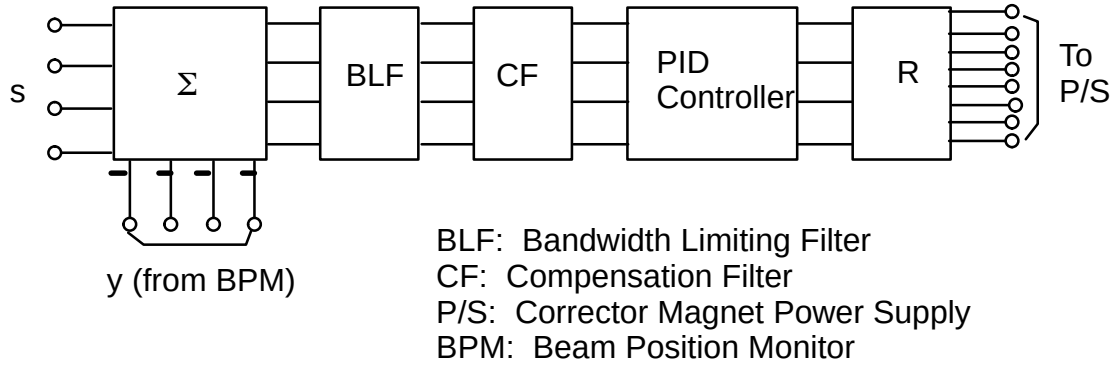

Fig. 4.1: Schematic of the global beam position feedback using DSP with the pseudo–inverting matrix R for M = 4 and N = 8. The controller gains are constant for all channels.

4.2 Local Feedback

The local feedback loops will employ four–magnet bumps to control both the position and the angle of the x–ray source point as shown in Fig. 4.2. For the bending magnet radiation, the source point is placed at the center of the main dipole, while for the insertion device, the radiation is along the extension of the line adjoining the beam position at the location of the bump magnets 2 and 3.

The position and the angle of the radiation source are monitored using a set of two x–ray photon beam position monitors at the end of the beam line, which register the photon beam positions (y_{b1} and y_{b2}) at longitudinal locations x_{b1} and x_{b2}. In the following discussion we will discuss the case of the insertion device radiation and will ignore for simplicity the effect of the vacuum chamber eddy current which results in local bump closure error. The case of the bending magnet radiation can be done in a similar manner. Consider the relation between the δ_a and δ_b, the strengths of the three–magnet bumps a and b, and the photon beam positions y_{b1} and y_{b2},[5]

$$\begin{pmatrix} \delta_a \\ \delta_b \end{pmatrix} = (\mathbf{DA})^{-1} \begin{pmatrix} y_{b1} \\ y_{b2} \end{pmatrix}, \tag{4.6}$$

where

$$A = \sqrt{\beta_2 \beta_3}\ \sin(\phi_3 - \phi_2) \begin{pmatrix} K_{3a} & 0 \\ 0 & K_{2b} \end{pmatrix} \tag{4.7}$$

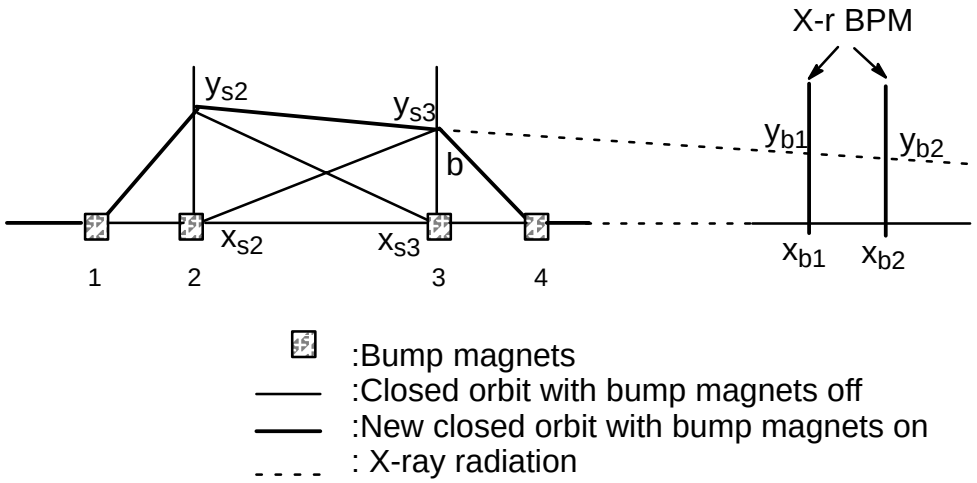

Fig. 4.2: Four–magnet bump to control the position and the angle of the x–ray radiation, which comprises the two three–magnet bumps a (magnets 1, 2, and 3) and b (magnets 2, 3, and 4). x and y are coordinates for the longitudinal distance and the beam position, respectively.

and

$$\mathbf{D} = \frac{1}{x_{s3} - x_{s2}} \begin{bmatrix} -|x_{b1} - x_{s3}| & |x_{b1} - x_{s2}| \\ -|x_{b2} - x_{s3}| & |x_{b2} - x_{s2}| \end{bmatrix}. \tag{4.8}$$

K_{3a} is the relative weight of the magnet 3 in the bump a, and K_{2b} is the relative weight of the magnet 2 in the bump b. β_2 and β_3 are the β–function values at the bump magnet locations 2 and 3, and ϕ_2 and ϕ_3 are the corresponding betatron phases. In order to have the bump closure, the relative weights K_{ij} (i=1,2,3, and j=a,b) must satisfy

$$\frac{K_{2a}}{K_{1a}} = -\sqrt{\frac{\beta_1}{\beta_2}}\,\frac{\sin(\phi_3 - \phi_1)}{\sin(\phi_3 - \phi_2)}, \qquad \frac{K_{3a}}{K_{1a}} = \sqrt{\frac{\beta_1}{\beta_3}}\,\frac{\sin(\phi_2 - \phi_1)}{\sin(\phi_3 - \phi_2)} \tag{4.9}$$

and

$$\frac{K_{3b}}{K_{2b}} = -\sqrt{\frac{\beta_2}{\beta_3}}\,\frac{\sin(\phi_4 - \phi_2)}{\sin(\phi_4 - \phi_3)}, \qquad \frac{K_{4b}}{K_{2b}} = \sqrt{\frac{\beta_2}{\beta_4}}\,\frac{\sin(\phi_3 - \phi_2)}{\sin(\phi_4 - \phi_3)} \tag{4.10}$$

Equation (4.6) relates the strength of the bump magnets and the photon beam motion and is the basis of the closed loop feedback. The schematic is shown in Fig. 4.3. The vector **s** is the control signal for the photon beam position vector **y** (y_{b1} and y_{b2}),

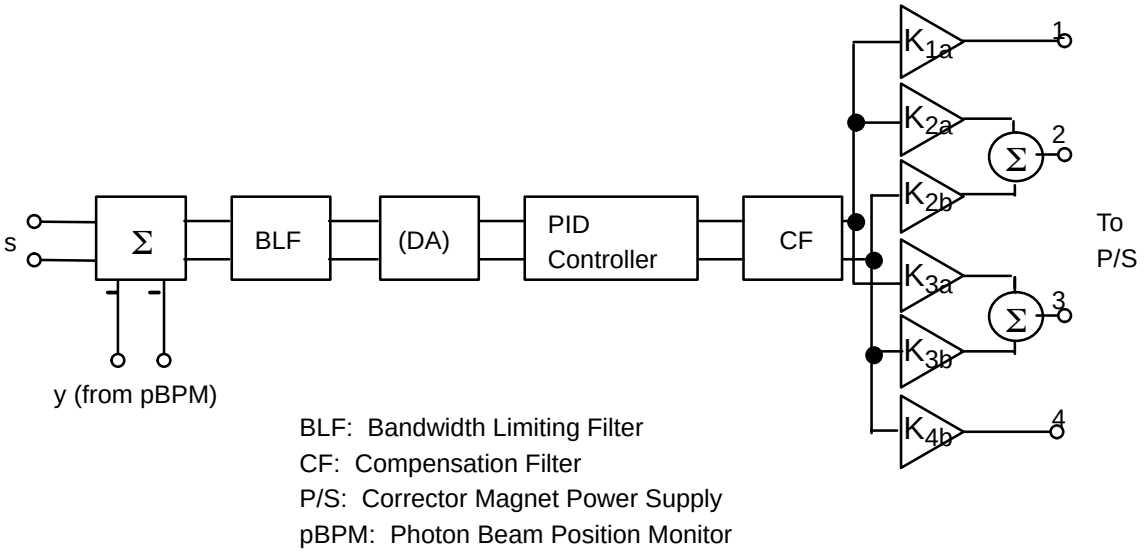

Fig. 4.3: Schematic of the local beam position feedback using DSP.

whose difference is fed to the digital signal processor. The output from the matrix $(\mathbf{DA})^{-1}$ is the three–magnet bump strength δ_a and δ_b, which is split to the four power supplies for the bump magnets.

5. Summary and Suggestions for Future Work

In this note, we reviewed formulation of digital signal processing based on Z–transforms and the PID control algorithm, and discussed its application to the global and local beam position feedback in the APS storage ring. The emphasis was on the compensation of the eddy current induced in the thick aluminum vaccum chamber of the APS storage ring by the corrector magnet field to cancel the external perturbation. The digital filter discussed in Section 2 for the compensation of the eddy current will not cover all frequencies. This non–ideal behavior will result in limitation of the controller gains (K_P, K_I, and K_D), high sampling frequency F_s, and reduced bandwidth of the feedback loop. The optimization of these parameters with a safety margin for stable operation requires measurement of the effect of the vacuum chamber eddy current up to 1 kHz (with F_s=4 kHz). More analytical studies on the PID control will also be needed.

The eddy current in the asymmetric vacuum chamber will also induce quadrupole and sextupole components in the magnetic field applied on the particle beams. Even though the quadrupole field can be minimized by symmetrizing the geometry, e.g., attaching a piece of the vacuum chamber cut from the photon exit channel to the antechamber, the sextupole component still remains. This will result in a bump closure error at the point of local correction, which may not be negligible in the frequency range (DC to 25 Hz) of our interest. A detailed discussion of this problem and its solution will be presented separately.

References

1. G. Decker, Y. Chung, and M. Kahana, “Progress on the Development of APS Beam Position Monitoring System,” Proceedings of the Particle Accelerator Conference, San Francisco, 1991

2. A. Peled and B. Liu, *Digital Signal Processing*, John Wiley & Sons, 1976

3. M. Sands, “The Physics of Electron Storage Rings – An Introduction,” SLAC–121 (1970)

4. W. Press et al., *Numerical Recipes in C*, Cambridge University Press, p. 60, 1989

5. S. Krinsky, et al. “Storage Ring Development at the National Synchrotron Light Source,” BNL–46615, p. 58, 1991